

Generating High-Precision Force Fields for Molecular Dynamics Simulations to Study Chemical Reaction Mechanisms using Molecular Configuration Transformer

Sihao Yuan, Xu Han, Zhaoxin Xie, Cheng Fan, Yi Issac Yang*, Yi Qin Gao*

Sihao Yuan, Institute of Theoretical and Computational Chemistry, College of Chemistry and Molecular Engineering, Peking University, Beijing 100871

Zhaoxin Xie, Institute of Theoretical and Computational Chemistry, College of Chemistry and Molecular Engineering, Peking University, Beijing 100871

Cheng Fan, Institute of Theoretical and Computational Chemistry, College of Chemistry and Molecular Engineering, Peking University, Beijing 100871

Xu Han, Institute of Theoretical and Computational Chemistry, College of Chemistry and Molecular Engineering, Peking University, Beijing 100871

Yi Isaac Yang, Institute of Systems and Physical Biology, Shenzhen Bay Laboratory, Shenzhen 518132
Email: yangyi@szbl.ac.cn

Yi Qin Gao, Institute of Theoretical and Computational Chemistry, College of Chemistry and Molecular Engineering, Peking University, Beijing 100871
Institute of Systems and Physical Biology, Shenzhen Bay Laboratory, Shenzhen 518132
Email: gaoyq@pku.edu.cn

Abstract

Theoretical studies on chemical reaction mechanisms have been crucial in organic chemistry. Traditionally, calculating the manually constructed molecular conformations of transition states for chemical reactions using quantum chemical calculations is the most commonly used method. However, this way is heavily dependent on individual experience and chemical intuition. In our previous study, we proposed a research paradigm that uses enhanced sampling in QM/MM molecular dynamics simulations to study chemical reactions. This approach can directly simulate the entire process of a chemical reaction. However, the computational speed limits the use of high-precision potential energy functions for simulations. To address this issue, we present a scheme for training high-precision force fields for molecular modeling using our developed graph-neural-network-based molecular model, molecular configuration transformer. This potential energy function allows for highly accurate simulations at a low computational cost, leading to

more precise calculations of the mechanism of chemical reactions. We have used this approach to study a Cope rearrangement reaction and a Carbonyl insertion reaction catalyzed by Manganese. This “AI+Physics” based simulation approach is expected to become a new trend in the theoretical study of organic chemical reaction mechanisms.

Introduction

The simulation of chemical reactions plays a crucial role in enhancing our understanding of both chemical and biological reactions. Various quantum mechanical calculation methods, such as the Hartree-Fock method, density functional methods, post-Hartree-Fock methods, etc.¹, can provide detailed potential energy surfaces and the corresponding electronic properties of molecular configurations. However, as the complexity of reaction systems increases, an increasing number of local minima in the configuration space and entropy effects from energetically similar configurations become more significant^{2,3}. Traditional methods based on single-point energy calculations have difficulty effectively traversing the entire configuration space, posing a risk of missing low-energy conformations⁴. Therefore, for such systems, molecular dynamics methods are an effective analytical tool.

Compared to chemical reaction studies based on single-point energy calculations, molecular dynamics simulations have the capability to directly consider temperature, entropy, kinetics, solvent effects, etc. They also possess the ability to explore reaction mechanisms independently of initial assumptions about reaction pathways^{3,5}. Additionally, chemical reactions, as a class of rare events, may occur on timescales of milliseconds or even longer, which can significantly differ from the simulation timescale. Enhanced sampling methods have been devised to overcome the timescale limitations of MD simulations, allowing for a more effective exploration of phase space⁶.

The metadynamics method is an enhanced sampling technique based on collective variables (CV)⁷. It achieves enhanced sampling by superimposing Gaussian potentials on collective variables, thereby smoothing out the energy differences between potential wells and barriers. A well-defined CV should describe the most difficult-to-sample degrees of freedom in a system and differentiate between its various stable states. The efficiency of the aforementioned enhanced sampling methods significantly relies on the quality of the defined CVs. Obtaining good CVs for complex systems can be challenging. For example, the reaction coordinates for transition-metal-catalyzed organic reactions can be complicated because of the participation of transition-metal centers and ligands. Harmonic Linear Discriminant Analysis (HLDA) is an effective method used to identify CVs^{8,9}. HLDA has demonstrated its effectiveness in various applications related to chemical reactions by generating CVs through linear combinations of provided descriptors without necessitating information about transition states^{10,11}.

The most commonly employed method for computing energy and forces in molecular simulations of reaction systems, i.e., the potential energy function, is presently the semi-empirical approach^{12–14}. Semi-empirical methods are also grounded in quantum mechanical principles. In semi-empirical methods, empirical parameters are employed in lieu of computationally expensive integrals, thereby enhancing computational speed. However,

this approach often compromises precision in certain chemically significant reaction systems, occasionally yielding erroneous outcomes. Furthermore, compared to classical force fields, semi-empirical methods still entail relatively high computational costs.

In recent years, deep neural networks have witnessed rapid development. Properly designed network architectures have proven adept at accurately describing systems and fitting potential energy surfaces, thereby enabling the generation of high-precision force fields for rapid computations. Examples of such models include BPNN¹⁵, ANI-1¹⁶, DPMD¹⁷, SchNet¹⁸, PhysNet¹⁹, among others. We opted for the graph-based Molecular Configuration Transformer (MolCT)²⁰ model, a GNN-based model.

With the increasing interest among chemical researchers in understanding reaction mechanisms, the diverse array of software available in the market varies in installation requirements and open-source availability, thereby complicating their usability. Moreover, not all individuals have undergone computational chemistry training, limiting their ability to proficiently navigate tasks such as finding CVs, identifying transition states, and employing enhanced sampling methods. In response to these needs, we have introduced an open-source workflow based on the Python platform. This workflow facilitates the entire process, starting from conformational sampling within reaction systems to fitting neural network force fields. It enables the extraction of dynamic properties related to reactions, including transition states, catering to individuals without extensive expertise in computational chemistry.

Methods

Using high-precision neural network potential energy surfaces to study chemical reactions typically involves the following steps:

1. **Conformational Sampling:** Thoroughly sample the conformational space of the system, often involving the selection of CVs and appropriate enhanced sampling methods. For systems where the reaction coordinates are not evident, we employ the Harmonic Linear Discriminant Analysis (HLDA) method. The HLDA method is an improvement of LDA (linear discriminant analysis) method specifically tailored for chemical reaction systems. It performs data dimensionality reduction, aiming to compact similar data types while dispersing different types as much as possible. In chemical reaction systems, the breaking and formation of bonds represent typical characteristics. Hence, we chose bond lengths as descriptors for the reaction CVs. Assuming that N_d descriptors $d(R)$ are needed for a chemical reaction in HLDA method, and the system as M stable states. The MD simulations from stable states are performed, and the configurations from each trajectory are considered as points in N_d -dimensional linear space defined by descriptor $d(R)$. The HLDA method separates these groups in a dimension-reduced space by a projection matrix W , yielding $M-1$ nonzero eigenvalues with corresponding eigenvectors, the coefficients of the linear combinations of descriptors as CVs.

After choosing CVs by the HLDA methods or observation, we perform semi-empirical simulation with Metadynamics enhanced sampling methods. For thorough sampling, the goal is to observe multiple interconversions between reactants and products, as well as various conformations around the transition state. In

this sampling process, it's possible to include constraints to prevent excessively high atomic energies that might lead to simulation crashes. Typically, achieving comprehensive sampling might require enhanced sampling simulations ranging from a few nanoseconds to several tens of nanoseconds.

2. Selection of Representative Configurations and Ab-initio Quantum Mechanical Calculations: Choose suitable configurations and conduct high-precision quantum mechanical calculations. Selecting representative conformations is crucial, especially in collecting densely populated points near high-energy transition states. To achieve this, retaining as many points as possible near the transition state from the trajectories obtained in the initial sampling phase is advisable. When the transition state is challenging to determine, conformations that are reasonable but possess higher potential energy can be considered for selection. Additionally, in sampling stable states, avoiding highly similar conformations can prevent unnecessary computational redundancy. These criteria for data selection also apply to supplementing data for less stable neural network force fields in the final section.

Perform high-precision quantum chemical calculations on the selected representative conformations to obtain their respective single-point energies and the negative gradients of energy, which represent the forces acting on each atom. This process generates a dataset containing atomic coordinates, energies, and forces for each conformation. The dataset is then subject to whitening procedures, which involve subtracting the reference energy of atoms computed at the same level, unit conversion, and normalization based on energy.

3. Neural Network Training: Train the neural network model using the obtained high-precision data. In our training task for energy and force, the loss function used is formulated as follows:

$$L = w_E \left(\frac{E^{\text{pred}}}{N_{\text{atoms}}} - \frac{E^{\text{label}}}{N_{\text{atoms}}} \right)^2 + \frac{w_F}{N_{\text{atoms}}} \sum_i^{N_{\text{atoms}}} \left(d_F F_i^{\text{pred}} - d_F F_i^{\text{label}} \right)^2$$
$$d_F = \frac{\sigma(E^{\text{label}})}{N_{\text{atoms}} |\text{mod}(F^{\text{label}})|}$$

This formulation ensures that the units of loss for both energy and force are consistent. Using force labels in the training dataset and loss function helps in obtaining an accurate force field and ensures the smoothness of the energy function.

4. Evaluation of Force Field: Assess the force field's performance to identify any unreasonable conformations it might produce. After sufficiently iteration of training, having low loss on the validation and test sets doesn't necessarily imply that the force field has learned comprehensively. It's essential to conduct dynamic simulations using this force field to evaluate its performance. The trained neural network force field was implemented into the MindSPONGE simulation package²¹ for molecular dynamics simulation. Ideally, applying bias potentials and restraint potentials similar to those used in the initial configuration sampling step should promote the occurrence of the reaction. If the simulation proceeds stably without structural collapse or unintended product generation, it indicates a well-represented force field for describing the chemical reaction. Otherwise, subsequent data augmentation and retraining might be necessary.

5. Utilization of Trained Discriminator: Employ the trained discriminator to identify configurations requiring re-computation and retrain the neural network accordingly. In the first step, we sampled conformations from the potential energy surface defined by semi-empirical methods and restraints we applied. However, when conducting molecular dynamics simulations using the trained network, the generated conformations may significantly differ from those obtained through semi-empirical methods. This discrepancy can extend beyond the range within which the neural network can accurately infer, leading to structural collapse or unintended product generation. Therefore, further data supplementation is required for refining the network.

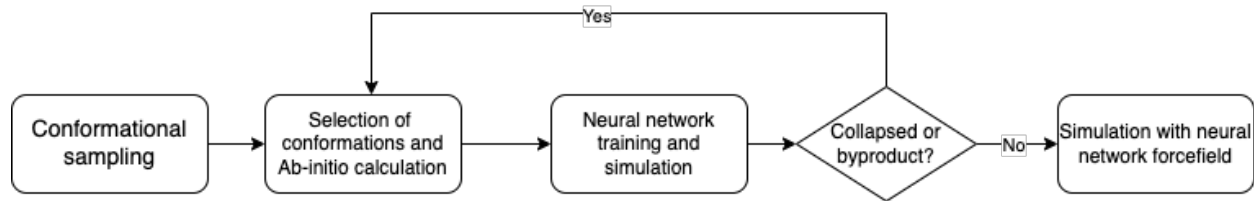
Addressing the challenge of supplementing new data presents a paradox: the new data should ideally be as dissimilar as possible from the original dataset to avoid redundancy and conserve computational resources. However, simultaneously, we seek new data that is chemically plausible—representing conformations likely to occur during simulations. Otherwise, acquiring such data not only incurs additional computational time but also contaminates the training set.

We draw inspiration from Generative Adversarial Networks (GANs)²². Structures obtained from semi-empirical simulations are considered as real samples (positive samples), while structures generated by the neural network force field serve as generated samples (negative samples). A molecule representation model is trained as a classifier to differentiate between these two categories as accurately as possible. This classifier employs a binary cross-entropy loss function,

$$L = -\frac{1}{N_{pos}} \sum_{N_{pos}} y_{pos} \log D(x_{pos}) - \frac{1}{N_{neg}} \sum_{N_{neg}} (1 - y_{neg}) \log (1 - D(x_{neg}))$$

where D represents the discriminative function desired in this study. Structures from semi-empirical simulations are labeled with $y_{pos} = 1$, while structures generated from the neural network force field simulations are labeled with $y_{neg} = 0$. Consequently, as the discriminative results for semi-empirical samples approach 1 and simultaneously approach 0 for neural network samples, the loss function diminishes. Then, we selected structures within a certain range of the discriminant function, greater than 0 and less than 1, as supplementary data. Repeating steps 2 through 5 until the neural network potential can stably perform molecular dynamics simulations of the chemical reaction.

The workflow is outlined in Scheme 1. These steps constitute a fundamental process when employing high-precision neural network potentials for chemical reaction studies. In our workflow, various methods are available for selection. During the conformational sampling phase, options include utilizing the MINDO3 method based on PySCF²³ or the AM1 method based on MindSpore in conjunction with Mindsponge's enhanced sampling capabilities. Additionally, one can employ built-in semi-empirical calculation methods in Amber²⁴ along with the Plumed²⁵ enhanced sampling plugin. For high-precision quantum chemical calculations, various computing packages like PySCF, Gaussian²⁶, ORCA²⁷, and others are also available.



Scheme 1. The overall flowchart of method.

Results

Cope rearrangement

We are simulating the intramolecular Cope rearrangement of *cis*-2-vinylcyclopropane carbaldehyde. The schematic diagram presented below depicts the selected reaction system, which involves the conversion between a seven-membered ring (referred to as molecule (A) and a three-membered ring (referred to as molecule (B)). Here, we have opted to employ the semi-empirical DFTB method for rapid conformational exploration of this system. All simulations were performed by SANDER in AMBER20 package patched with PLUMED2. In a non-periodic boundary box, Langevin thermostat with a friction coefficient of 5.0 ps^{-1} was employed to conduct a 4-walker simulation at 800K, with a time step of 1 fs and 10ns each. Utilizing the Metadynamics technique for enhanced sampling, the collective variable is defined as the difference between bond formation and bond breaking distances, represented as $d_6 - d_3$. The height of Gaussian function was 1 kJ/mol, and the bias factor γ was 100. The Gaussian sigma was 0.01 for the CV. In addition, to avoid unwanted byproducts, additional restraints were added to the system. For more details, please refer to Supporting Information. The free energies were obtained by a reweighting procedure considering all restraints.

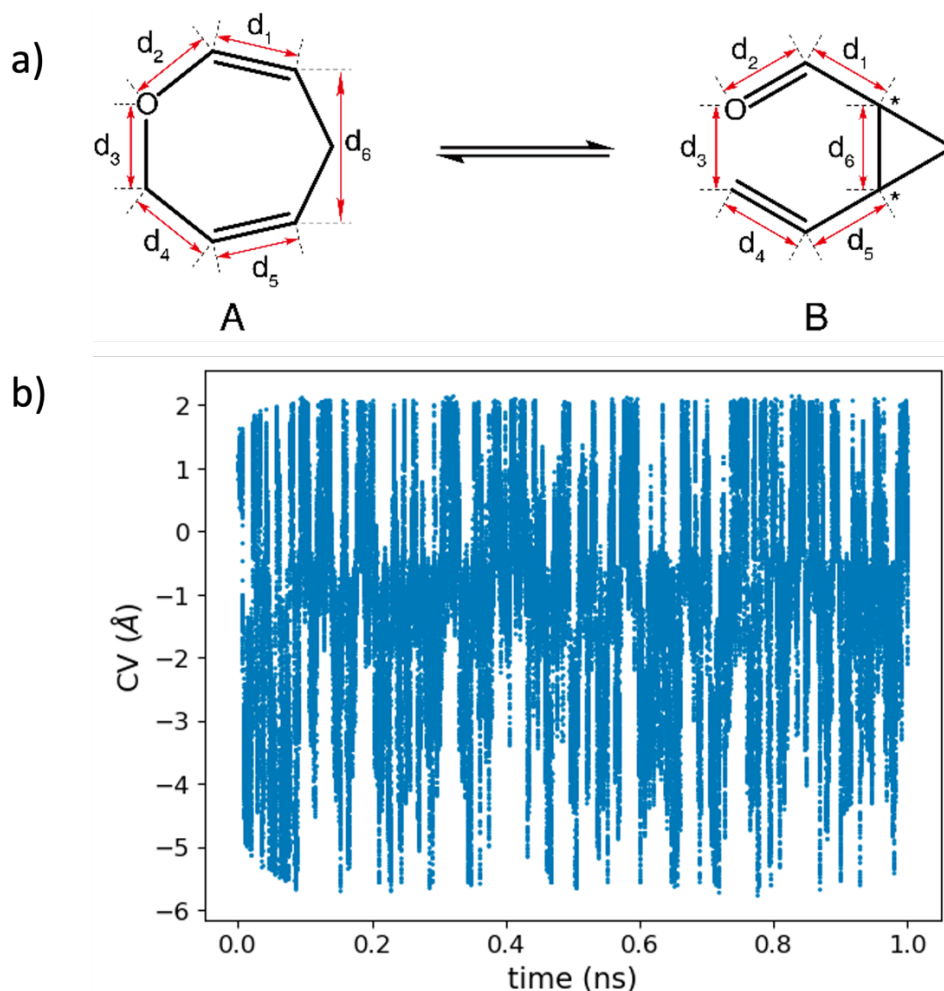


Figure 1. a) The illustration of Cope rearrangement and the definition of distances between atoms. b) CV evolution of DFTB sampling with simulation time.

After sufficiently sampling molecular conformations, we retained configurations with CVs ranging from -0.05nm to 0.05nm, while other configurations were uniformly sampled along the CV, resulting in a total of 133,120 samples. As depicted in the graph, the dataset is approximately uniformly distributed along the reaction CV, encompassing the majority of transition state structures. Subsequently, quantum chemical computations were conducted at the B3LYP/6-31+G** level with Gaussian package. The dataset was randomly partitioned into a training set of 131,072, a validation set of 1,024, and a test set of 1,024 conformations.

Due to the relatively large numerical values obtained from quantum chemical computations of single-point energies, it is often necessary to first subtract a reference energy. The reference energy is typically the sum of single-point energies calculated for individual atoms using the same method. Employing the B3LYP method and the 6-31+G** basis set, the energies calculated for individual carbon (C), hydrogen (H), and oxygen (O) atoms were found to be -0.496862, -37.762005, and -74.935438 Ha, respectively. These energies are subtracted from the total single-point energy to obtain corrected values.

The training was conducted with a cutoff of 1 nm, utilizing 3 interaction layers, a feature dimensionality of 128, and 8 attention heads. The training spanned 500 epochs, it is evident that the loss rapidly converged according to supp. fig. 1.

The trained force field was tested and compared with the force and energy obtained using the semi-empirical method. It was observed that our trained force field aligns with chemical accuracy within the sampled conformational space. In comparison to the semi-empirical method, the neural network force field demonstrates superior performance in terms of energy and force (figure 2 and Supp fig 2). The configurations of the seven-membered ring predominantly occupy lower-energy regions, while the three-membered ring configurations tend to reside in higher-energy areas. Additionally, the sparser configurations with the highest energy correspond to transition state conformations.

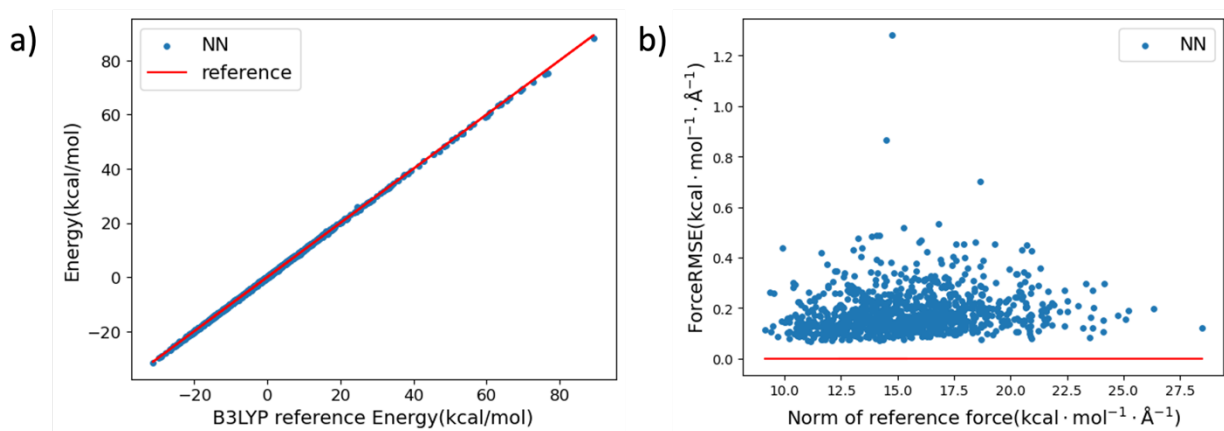


Figure 2. a) Energy evaluation on testing set. b) Force root mean square error (RMSE) on testing set.

The simulation was conducted at a temperature of 800K with a timestep of 1fs, spanning a duration of 300ps. Metadynamics was employed for enhanced sampling along the previously defined CV, utilizing the same settings as described earlier. This setup facilitated the observation of interconversion between reactants and products. However, the system collapsed after 250ps (Supp fig 3).

We ran 100 trajectories in parallel, each for 300ps. Along these trajectories, 996 points were randomly selected uniformly based on the CV to evaluate the performance of energy and force predictions during the dynamic simulations. Among these, 9 points exhibited non-convergence during the SCF calculations, while several points showed abnormally high energies. There are two kinds of unwanted high energy structures. One presented clash between H atom and C atom, the other is produces two fragments of the molecule. For structures with normal energies, there are also some points showing significantly high Mean Squared Error (MSE) in forces. These structures fall into two categories: one with excessively elongated carbon-carbon bonds, and the other in the vicinity of the transition state.

We selected points near the structures exhibiting similar characteristics as described earlier from the trajectories

generated by the neural network force field. Subsequently, these additional 7734 data points were included alongside the randomly selected half of the original dataset, resulting in a total of 84349 data points. This expanded dataset was partitioned into 83197 for the training set, 128 for the validation set, and 1024 for the test set. The retrained network exhibited convergence in loss, while the errors in energy and force aligned within chemical accuracy (supp. fig. 5).

We conducted simulations using the new network with 100 parallel runs, each lasting 500ps, maintaining consistent parameters as before. Subsequently, performing B3LYP/6/31+G** calculations on the sampled points derived from these simulations, we evaluated the energy differences between the predicted energies by the neural network and B3LYP. This allowed us to obtain the "bias potential" of the neural network potential relative to the B3LYP energy after reweighting, which in turn provided the B3LYP/6/31+G** level free energy surface (FES).

Upon treating the DFB-sampled FES, a comparison between the two reveals significant differences in the DFTB-derived FES and reference FES (figure 3). Particularly, discrepancies were noted in the relative energies of Configuration A (right-side potential well on FES) and Configuration B (left-side potential well on FES). The DFTB-derived FES suggests that Configuration A has lower free energy compared to Configuration B, contrary to the actual expected result where Configuration B should have lower free energy than Configuration A.

On the other hand, the differences observed in the neural network potential's free energy surface before and after reweighting were minimal, reaching a maximum of only 5 kJ/mol. This emphasizes the importance of employing a higher-precision force field for sampling.

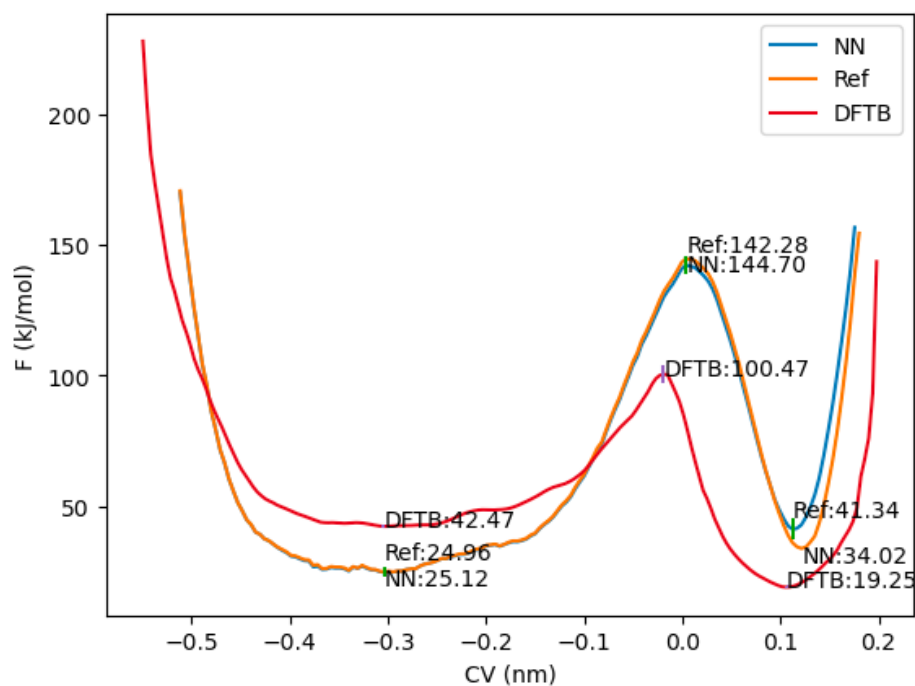


Figure 3. The free energy surface (FES) obtained from neural network potential, DFTB method and reference

FES.

Carbonyl insertion reaction catalyzed by manganese

Alkyl migration reactions represent fundamental organometallic reactions involving transition metals. Figure 4(a) illustrates a simple example wherein $\text{Mn}(\text{CO})_5\text{CH}_3$ reacts with carbon monoxide, resulting in the migration of a methyl group to a carbonyl moiety, producing $\text{Mn}(\text{CO})_5(\text{COCH}_3)$. This reaction is also commonly referred to as carbonyl insertion²⁸.

This reaction consists of two steps: the first involves the migration of a methyl group to the carbonyl moiety, while the second step involves the coordination of an external carbonyl group to the central manganese atom²⁹. This study focuses on simulating the first step, specifically the process of methyl group migration (figure 4b).

This study is conducted using the Amber20+plumed2 software suite. Initially, the HLDA algorithm was employed to explore the reaction coordinates. Due to the relative simplicity of this reaction, only two bond lengths, as depicted in figure 4(b), were chosen as descriptors for the HLDA algorithm. Molecular dynamics simulations of 300 ps were performed for both reactants and products using the PM6 semi-empirical method. The simulations were conducted at a controlled temperature of 300K, employing a Langevin thermostat with a friction coefficient (γ_{ln}) set to 1 ps^{-1} .

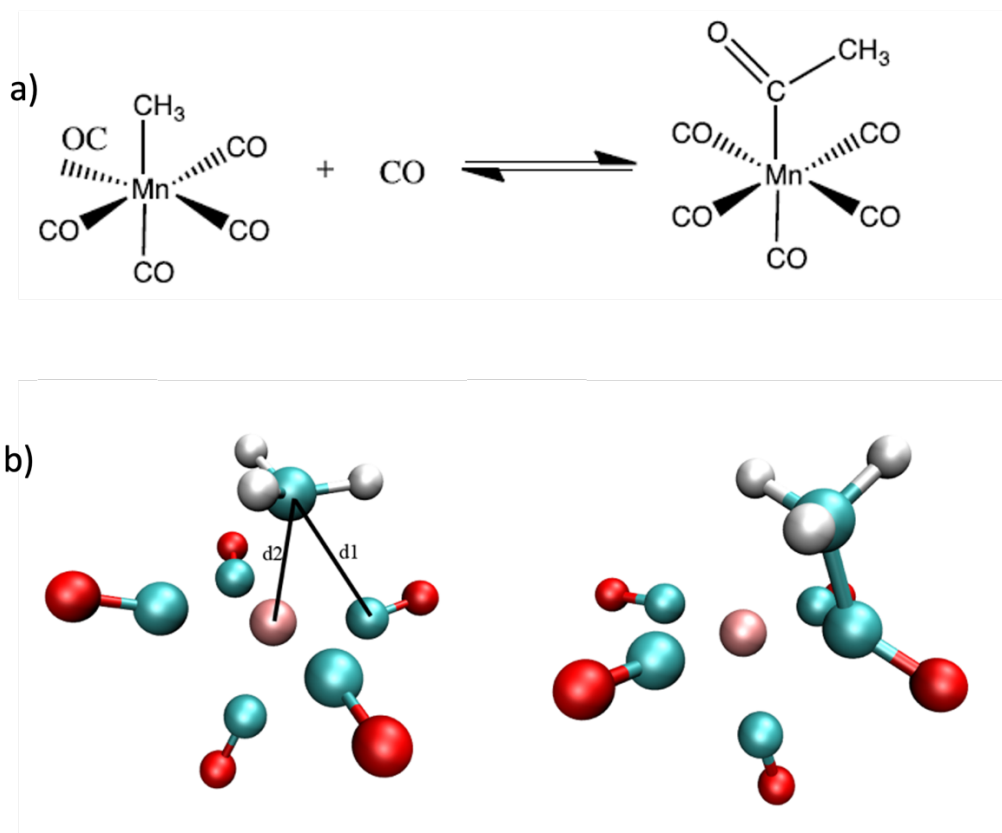


Figure 4. a) The carbonyl insertion reaction. b) The illustration of defined distance and the product.

Results from the HLDA algorithm reveal the collective variable (CV) as $CV = 0.99d1 + 0.14d2$. This indicates that the impending formation of the carbon-carbon bond holds an overwhelmingly dominant role in this process.

Subsequently, employing metadynamics, four parallel trajectories were simulated, each spanning 5 ns. The Gaussian hill parameters were set at a width of 0.01, a height of 1 kJ/mol, and a bias factor γ of 50, with other parameters remaining consistent with the aforementioned settings. As illustrated in figure 5, both reactants and products were observed to successfully interconvert.

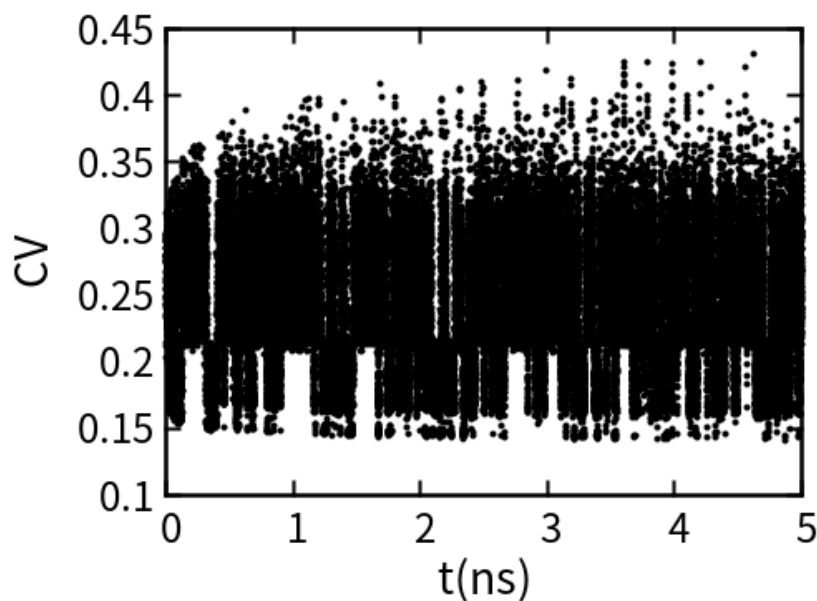


Figure 5. CV evolution of PM6 sampling with simulation time.

Under the PM6 level of accuracy, the computed free energy surface significantly deviates from the anticipated outcomes. Contrary to expectations, the intermediate generated in the first step exhibits an energy lower than that of the reactants, contrary to the expected higher energy state. Randomly selecting 200 structures from the trajectory, single-point energy calculations were performed using quantum chemical software ORCA 4.2.1 at the B3LYP/6-311++G** level, providing a comparative analysis against the PM6 results. The energy discrepancy between the two methods reaches up to 20 kcal/mol, a margin far beyond the bounds of chemical accuracy (supp. fig. 4). Therefore, the use of a higher-precision potential is imperative for conducting simulations.

Utilizing metadynamics sampling, a total of 167,704 structures were selected, comprising transition states, reactants, and products. Structures within the range of $d1$ between 1.73 to 1.87 Å were categorized as transition states (supp. fig. 5). Due to the sparsity of samples near the transition state, all 76,743 structures within this range were included. Random sampling was conducted for both reactant and product structures, resulting in the selection of 46,028 reactant structures and 44,933 product structures.

Using ORCA, calculations were performed for these structures at the B3LYP/6-311++G** level, obtaining the energy of the system along with the negative gradient energies, representing forces acting on individual atoms. From these results, 131,072 structures were selected for the training set, 1,024 for the validation set, and another 1,024 for the test set. Following 512 rounds of training, as depicted in supp. fig. 8, the system's loss has essentially converged. The mean absolute error for energy has reduced to below 0.5 kcal/mol, while the mean absolute error for force has diminished to below $0.2 \text{ kcal} \cdot \text{mol}^{-1} \cdot \text{\AA}^{-1}$, achieving chemical accuracy.

Utilizing the well-trained neural network, simulations were conducted on the molecular simulation platform Mindsponge using metadynamics. The simulation duration for this study was 0.1 ns with a timestep of 1 fs. The parameters for metadynamics included a Gaussian hill width of 0.01, a height of 10 kcal/mol, and a bias factor of 6. The metadynamics bias potential was updated every 100 steps, and coordinates were saved every 10 steps, resulting in 10,000 structures for each trajectory.

As illustrated in figure 6(a), the system maintained stability for a certain period. However, undesired conformations continued to emerge throughout the simulation until system collapse. For instance, at 0.02 ns, the coordination position of the carbon atom had deviated from the normal structure. At 0.04 ns, a byproduct emerged, where both the carbon atom from the carbonyl group and the oxygen atom simultaneously coordinated with the central manganese atom. Subsequently, chemically unexpected products appeared, such as a direct connection between a methyl hydrogen atom and the carbonyl group.

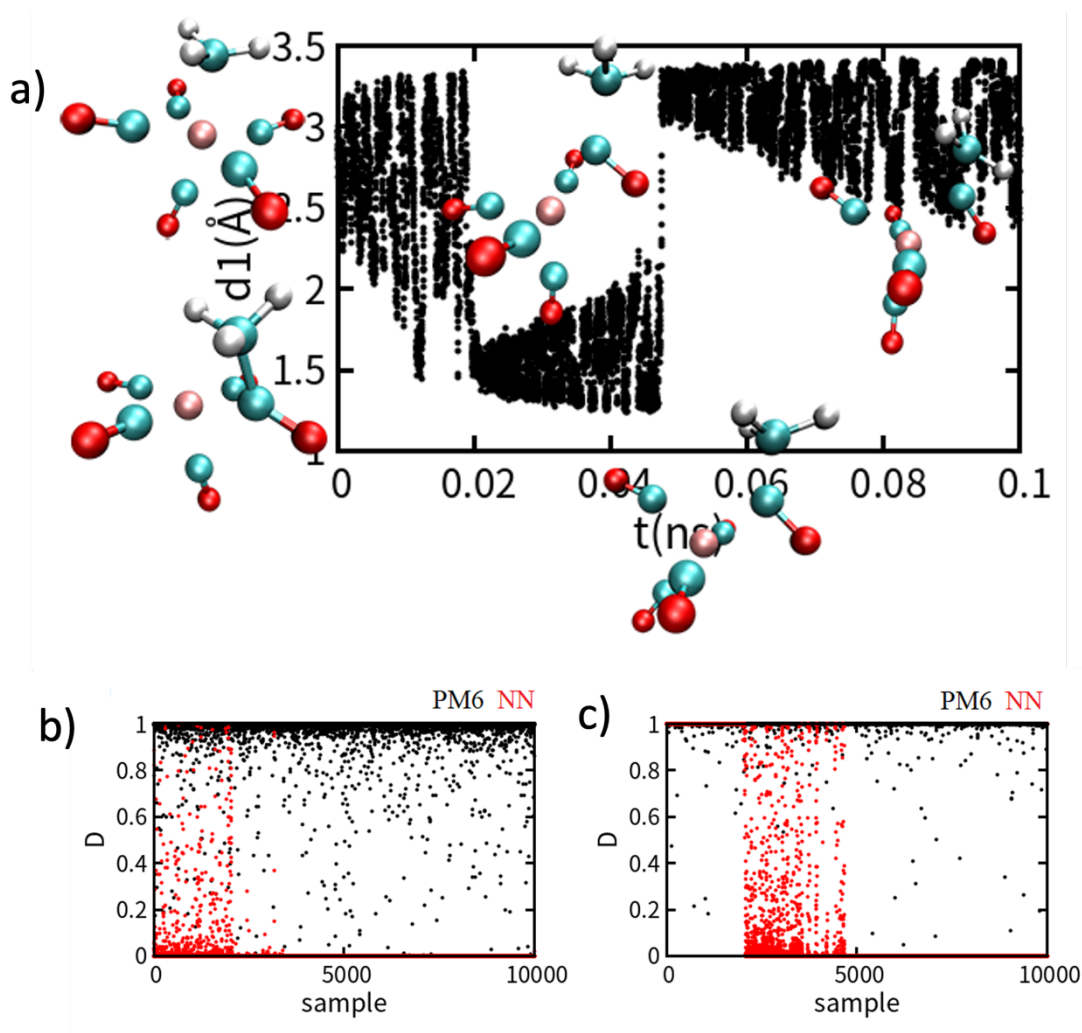


Figure 6. a) The trajectory generated by the neural network forcefield. b) and c) The classification function of conformations in NN-generated trajectory given by discriminator trained from b) all conformations in NN-generated trajectory c) collapsed conformations in NN-generated trajectory.

Positive samples can directly utilize the training set obtained from the first potential energy surface training. However, negative samples present different choices: either using all structures from the neural network or utilizing structures after system collapse. As depicted in figure 6(b), training using all structures from the neural network as negative samples demonstrates some structures with non-zero discriminative function (D) before the emergence of byproducts. However, after the appearance of byproducts, almost all structures exhibit D close to 0. This selection method limits the choice of data supplementation to only normal structures.

Alternatively, employing structures after system collapse as negative samples demonstrates that when the system is in a normal state (figure 6(c)), all structures exhibit D close to 1. Upon the appearance of byproducts, most structures exhibit D close to 0, and structures after system collapse show D close to 0 entirely. Consequently, this method primarily selects structures of the byproducts for data supplementation. Upon accurate energy and

force calculations for these byproducts, their generation can be avoided, potentially preventing system collapse. Hence, we opt for the latter method, utilizing structures after system collapse as negative samples.

We simulated 200 trajectories using the parameters mentioned earlier, resulting in a total of 2 million structures. We computed the discriminative function for these structures. Subsequently, 95,096 structures within the discriminative function range of 0.2 to 0.999 were selected for DFT calculations to supplement the dataset. Among these structures, 88,769 converged successfully. However, a subset of structures exhibited remarkably high energies (supp. fig. 6(a)), indicating their infeasibility.

Further analysis (supp. fig. 6(b)) revealed that the majority of structures concentrated below -2210 kcal/mol. Hence, we opted to include 61,516 structures with energies below -2210 kcal/mol as supplementary data. Consequently, over 60% of the quantified computational results were deemed valid.

The second round of training was conducted on the new dataset. As depicted in supp. fig. 10, the system's loss also converged, with the errors in force and energy maintained within the bounds of chemical accuracy.

The obtained neural network potential energy was utilized for conducting metadynamics simulations for 1 ns, with a simulation time step of 1 fs. The metadynamics parameters included a Gaussian peak width of 0.01, a height of 1 kcal/mol, and a bias factor of 50. As depicted in supp. fig. 7, during the 1 ns simulation, the system successfully demonstrated mutual interconversion between reactants and products. Moreover, this transition between reactants and products occurred without significant hindrance, implying the absence of distinct energy barriers segregating reactants from products throughout the simulation.

We continued the simulation for an additional 1 ns with the fixed metadynamics bias potential and constructed the free energy surface (FES) for this reaction based on the data obtained from this extended simulation. Additionally, using the PM6 semi-empirical method, we also plotted the FES for this reaction (figure 7). Under PM6 precision, the free energy of the transition state is notably higher than that of the reactants and products. However, on the neural network potential energy surface, the free energy of the transition state closely resembles that of the product. By comparing with reported single-point energy calculations in the literature, it is evident that the neural network potential energy surface effectively reproduces the accuracy of the DFT-level potential energy surface.

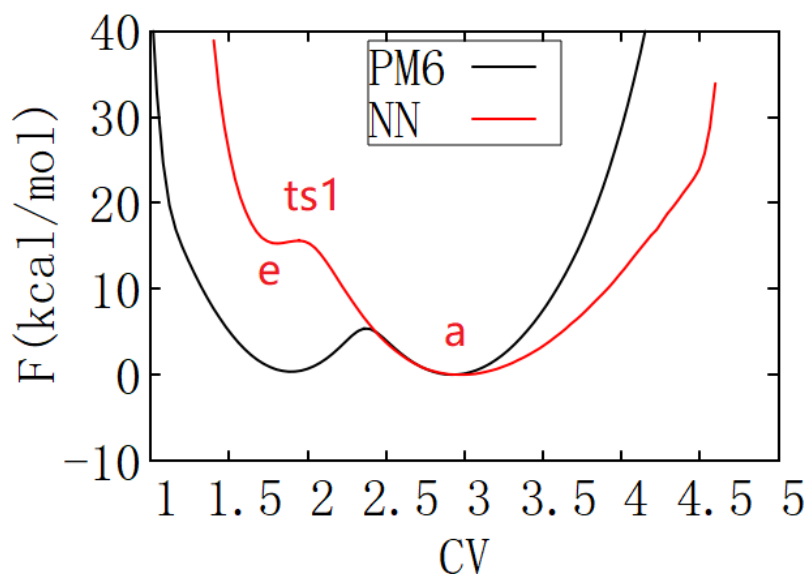


Figure 7. The FES of first step of carbonyl insertion reaction obtained from NN forcefield and PM6 method. The energy gap from NN between e-a and ts1-a is 15.3 kcal/mol and 15.6 kcal/mol, respectively. The reported value is 14.4 kcal/mol and 14.5 kcal/mol²⁹. PM6 got a qualitatively wrong FES.

Conclusion

In this study, we merged enhanced sampling methodologies with deep learning techniques, applying them to investigate the reaction mechanisms of the Cope rearrangement and manganese carbonyl insertion reactions. In the simulation of Cope rearrangement, we found that DFTB method might give incorrect free energy difference between two conformations. This might come from the flexibility of conformation (B). And in the simulation of carbonyl insertion catalyzed by Manganese, e obtained free energy surfaces that aligned well with high-precision quantum chemical calculations, while PM6 method derived a free energy surface far from the literature report. For these chemical reaction systems, semi-empirical methods both exhibited accuracy limitations. By employing these two reactions, we demonstrated that our method allows for simulations and studies of reactions using potential energy surfaces at the high-precision ab initio level.

We aim to further explore more chemical reaction mechanisms using this methodology. Transition-metal-catalyzed organic reactions are important in biochemical studies³⁰ and industrial applications³¹. As we demonstrated in studies on carbonyl insertion, the semi-empirical parameters for transition metal are sometimes poor-behaving. We hope this simulation approach to expand the field of molecular dynamics study of reactions. Our next objective is to incorporate the influence of solvents or protein environments into the neural network force field, enabling it to account for environmental information. This step will further expand the scope of high-precision molecular dynamics studies.

Acknowledgment

The authors thank Yijie Xia and Yanheng Li for useful discussion. Computational resources were supported by Shenzhen Bay Laboratory supercomputing center. This work was supported by National Key R&D Program of China (No. 2022ZD0115003), National Natural Science Foundation of China (22003042, 22273061 to Y.I.Y., and 22050003, 92053202, 21821004, 21927901 to Y.Q.G.),

Reference

- (1) Lewars, E. G.; Lewars, E. G. Computational Chemistry: Introduction to the Theory and Applications of Molecular and Quantum Mechanics. *Computational Chemistry: Introduction to the Theory and Applications of Molecular and Quantum Mechanics* **2011**, 391–444.
- (2) Yang, Y.-F.; Cheng, G.-J.; Liu, P.; Leow, D.; Sun, T.-Y.; Chen, P.; Zhang, X.; Yu, J.-Q.; Wu, Y.-D.; Houk, K. N. Palladium-Catalyzed Meta-Selective C–H Bond Activation with a Nitrile-Containing Template: Computational Study on Mechanism and Origins of Selectivity. *Journal of the American Chemical Society* **2014**, *136* (1), 344–355.
- (3) Zhang, J.; Yang, Y. I.; Yang, L.; Gao, Y. Q. Conformational Preadjustment in Aqueous Claisen Rearrangement Revealed by SITS-QM/MM MD Simulations. *J. Phys. Chem. B* **2015**, *119* (17), 5518–5530. <https://doi.org/10.1021/jp511057f>.
- (4) Zhang, L.; An, K.; Wang, Y.; Wu, Y.-D.; Zhang, X.; Yu, Z.-X.; He, W. A Combined Computational and Experimental Study of Rh-Catalyzed C–H Silylation with Silacyclobutanes: Insights Leading to a More Efficient Catalyst System. *Journal of the American Chemical Society* **2021**, *143* (9), 3571–3582.
- (5) Lei, Y. K.; Zhang, J.; Zhang, Z.; Gao, Y. Q. Dynamic Electric Field Complicates Chemical Reactions in Solutions. *The Journal of Physical Chemistry Letters* **2019**, *10* (11), 2991–2997.
- (6) Yang, Y. I.; Shao, Q.; Zhang, J.; Yang, L.; Gao, Y. Q. Enhanced Sampling in Molecular Dynamics. *The Journal of chemical physics* **2019**, *151* (7).
- (7) Laio, A.; Parrinello, M. Escaping Free-Energy Minima. *Proceedings of the national academy of sciences* **2002**, *99* (20), 12562–12566.
- (8) Mendels, D.; Piccini, G.; Parrinello, M. Collective Variables from Local Fluctuations. *The journal of physical chemistry letters* **2018**, *9* (11), 2776–2781.
- (9) Piccini, G.; Mendels, D.; Parrinello, M. Metadynamics with Discriminants: A Tool for Understanding Chemistry. *Journal of chemical theory and computation* **2018**, *14* (10), 5040–5044.
- (10) Danese, M.; Bon, M.; Piccini, G.; Passerone, D. The Reaction Mechanism of the Azide–Alkyne Huisgen Cycloaddition. *Physical Chemistry Chemical Physics* **2019**, *21* (35), 19281–19287.
- (11) Ponte, F.; Piccini, G.; Sicilia, E.; Parrinello, M. A Metadynamics Perspective on the Reduction Mechanism of the Pt (IV) Asplatin Prodrug. *Journal of Computational Chemistry* **2020**, *41* (4), 290–294.
- (12) Elstner, M. The SCC-DFTB Method and Its Application to Biological Systems. *Theoretical Chemistry Accounts* **2006**, *116*, 316–325.
- (13) Stewart, J. J. Application of the PM6 Method to Modeling Proteins. *Journal of molecular modeling* **2009**, *15* (7), 765–805.
- (14) Dewar, M. J.; Zoebisch, E. G.; Healy, E. F.; Stewart, J. J. Development and Use of Quantum Mechanical

- Molecular Models. 76. AM1: A New General Purpose Quantum Mechanical Molecular Model. *Journal of the American Chemical Society* **1985**, *107* (13), 3902–3909.
- (15) Behler, J.; Parrinello, M. Generalized Neural-Network Representation of High-Dimensional Potential-Energy Surfaces. *Phys. Rev. Lett.* **2007**, *98*, 146401.
- (16) S. Smith, J.; Isayev, O.; E. Roitberg, A. ANI-1: An Extensible Neural Network Potential with DFT Accuracy at Force Field Computational Cost. *Chemical Science* **2017**, *8* (4), 3192–3203. <https://doi.org/10.1039/C6SC05720A>.
- (17) Zhang, L.; Han, J.; Wang, H.; Car, R.; Weinan, E. Deep Potential Molecular Dynamics: A Scalable Model With The Accuracy Of Quantum Mechanics. *Phys. Rev. Lett.* **2018**, *120*, 143001.
- (18) Schütt, K. T.; Sauceda, H. E.; Kindermans, P.-J.; Tkatchenko, A.; Müller, K.-R. SchNet – A Deep Learning Architecture For Molecules And Materials. *J. Chem. Phys.* **2018**, *148*, 241722.
- (19) Unke, O. T.; Meuwly, M. PhysNet: A Neural Network for Predicting Energies, Forces, Dipole Moments, and Partial Charges. *J. Chem. Theory Comput.* **2019**, *15*, 3678.
- (20) Zhang, J.; Zhou, Y.; Lei, Y.-K.; Yang, Y. I.; Gao, Y. Q. *Molecular CT: Unifying Geometry and Representation Learning for Molecules at Different Scales*. arXiv.org. <https://arxiv.org/abs/2012.11816v2> (accessed 2023-10-10).
- (21) Zhang, J.; Chen, D.; Xia, Y.; Huang, Y.-P.; Lin, X.; Han, X.; Ni, N.; Wang, Z.; Yu, F.; Yang, L.; Yang, Y. I.; Gao, Y. Q. Artificial Intelligence Enhanced Molecular Simulations. *J. Chem. Theory Comput.* **2023**, *19* (14), 4338–4350. <https://doi.org/10.1021/acs.jctc.3c00214>.
- (22) Goodfellow, I.; Pouget-Abadie, J.; Mirza, M.; Xu, B.; Warde-Farley, D.; Ozair, S.; Courville, A.; Bengio, Y. Generative Adversarial Nets. *Advances in Neural Information Processing Systems* **2014**, 2672.
- (23) Sun, Q.; Berkelbach, T. C.; Blunt, N. S.; Booth, G. H.; Guo, S.; Li, Z.; Liu, J.; McClain, J. D.; Sayfutyarova, E. R.; Sharma, S. PySCF: The Python-based Simulations of Chemistry Framework. *Wiley Interdisciplinary Reviews: Computational Molecular Science* **2018**, *8* (1), e1340.
- (24) Pearlman, D. A.; Case, D. A.; Caldwell, J. W.; Ross, W. S.; Cheatham III, T. E.; DeBolt, S.; Ferguson, D.; Seibel, G.; Kollman, P. AMBER, a Package of Computer Programs for Applying Molecular Mechanics, Normal Mode Analysis, Molecular Dynamics and Free Energy Calculations to Simulate the Structural and Energetic Properties of Molecules. *Computer Physics Communications* **1995**, *91* (1–3), 1–41.
- (25) Bonomi, M.; Branduardi, D.; Bussi, G.; Camilloni, C.; Provasi, D.; Raiteri, P.; Donadio, D.; Marinelli, F.; Pietrucci, F.; Broglia, R. A. PLUMED: A Portable Plugin for Free-Energy Calculations with Molecular Dynamics. *Computer Physics Communications* **2009**, *180* (10), 1961–1972.
- (26) Frisch, M. ea; Trucks, G. W.; Schlegel, H. B.; Scuseria, G. E.; Robb, M. A.; Cheeseman, J. R.; Scalmani, G.; Barone, V.; Petersson, G. A.; Nakatsuji, H. *Gaussian 16, Revision C. 01*; Gaussian, Inc., Wallingford CT, 2016.
- (27) Neese, F. The ORCA Program System. *Wiley Interdisciplinary Reviews: Computational Molecular Science* **2012**, *2* (1), 73–78.
- (28) Tanjaroon, C.; Zhou, Z.; Mills, D.; Keck, K.; Kukolich, S. G. Microwave Spectra and Theoretical Calculations for Two Structural Isomers of Methylmanganese Pentacarbonyl. *Inorganic chemistry* **2020**, *59* (9), 6432–6438.
- (29) Derecskei-Kovacs, A.; Marynick, D. S. A New Look at an Old Reaction: The Potential Energy Surface for the Thermal Carbonylation of Mn (CO) 5CH3. The Role of Two Energetically Competitive Intermediates

on the Reaction Surface, and Comments on the Photodecarbonylation of Mn (CO) ₅ (COCH₃). *Journal of the American Chemical Society* **2000**, *122* (9), 2078–2086.

- (30) Wu, R.; Xie, H.; Cao, Z.; Mo, Y. Combined Quantum Mechanics/Molecular Mechanics Study on the Reversible Isomerization of Glucose and Fructose Catalyzed by *Pyrococcus Furiosus* Phosphoglucose Isomerase. *J. Am. Chem. Soc.* **2008**, *130* (22), 7022–7031. <https://doi.org/10.1021/ja710633c>.
- (31) Han, X.; Sun, T.-Y.; Yang, Y. I.; Zhang, J.; Qiu, J.; Xiong, Z.; Qiao, N.; Wu, Y.-D.; Gao, Y. Q. Enhanced Sampling Simulations on Transition-Metal-Catalyzed Organic Reactions: Zirconocene-Catalyzed Propylene Polymerization and Sharpless Epoxidation. *CCS Chemistry* **2023**, 1–12.